*Electronic supplementary information*

# First-Principles Investigation of Two-Dimensional Covalent Organic Frameworks Electrocatalysts for Oxygen Evolution/Reduction and Hydrogen Evolution Reactions†

Jing Ji,[a] Cunjin Zhang,[a] Shuaibo Qin,[a] and Peng Jin*[ab]

[a]School of Materials Science and Engineering, Hebei University of Technology, Tianjin 300130, China. *E-mail:* china.peng.jin@gmail.com

[b]Key Laboratory of Special Functional Materials for Ecological Environment and Information (Hebei University of Technology), Ministry of Education, Tianjin 300130, China.

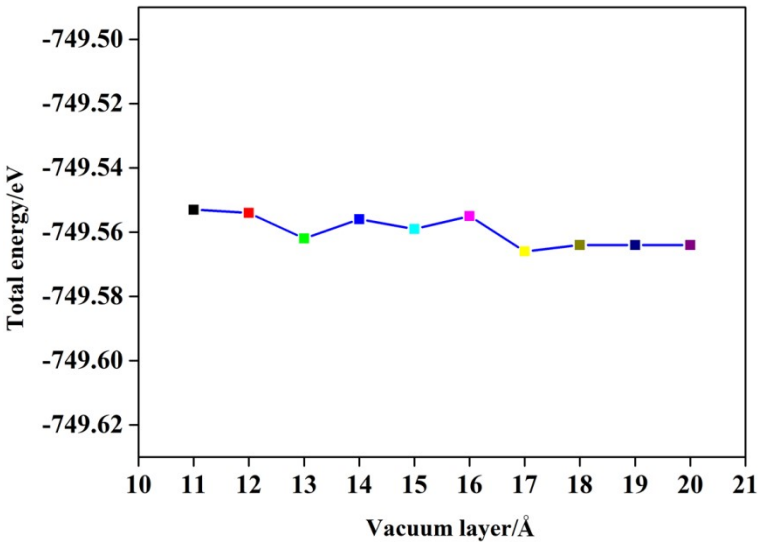


**Fig. S1** Calculated total energies of Co-COF as a function of the thickness of vacuum layer (11-20 Å). According to the small energy change (< 0.013 eV), a 15 Å vacuum layer is large enough for current study.

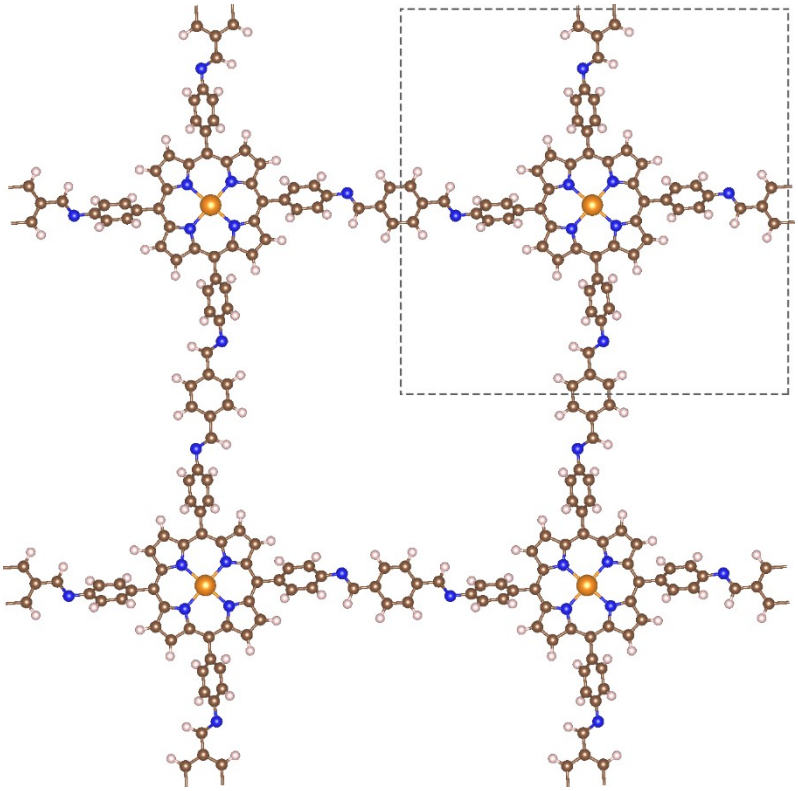

**Fig. S2** Unit cell (highlighted by the dashed line) used in the calculations of M-COFs (8 N atoms, 60 C atoms, 36 H atoms, and 1 metal atom). C: brown; N: blue; H: white; M: golden.

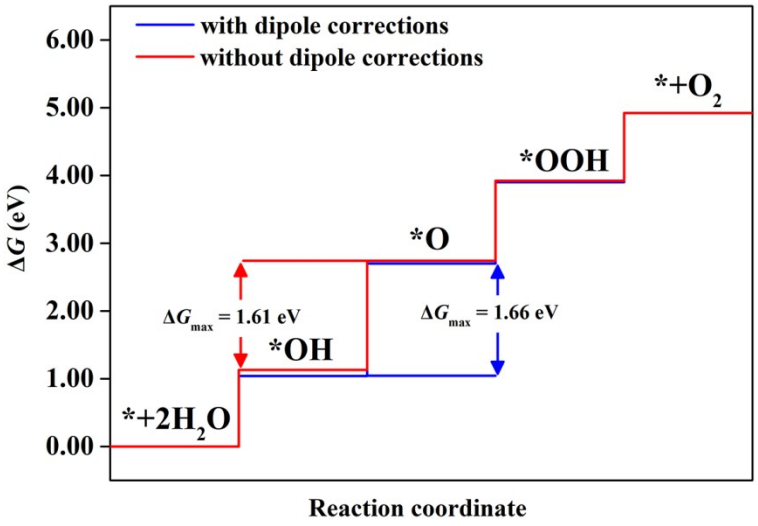


**Fig. S3** Gibbs free energy diagrams for the OER on Co-COF with and without dipole corrections. According to the small effect, the corrections were not considered in the current work.

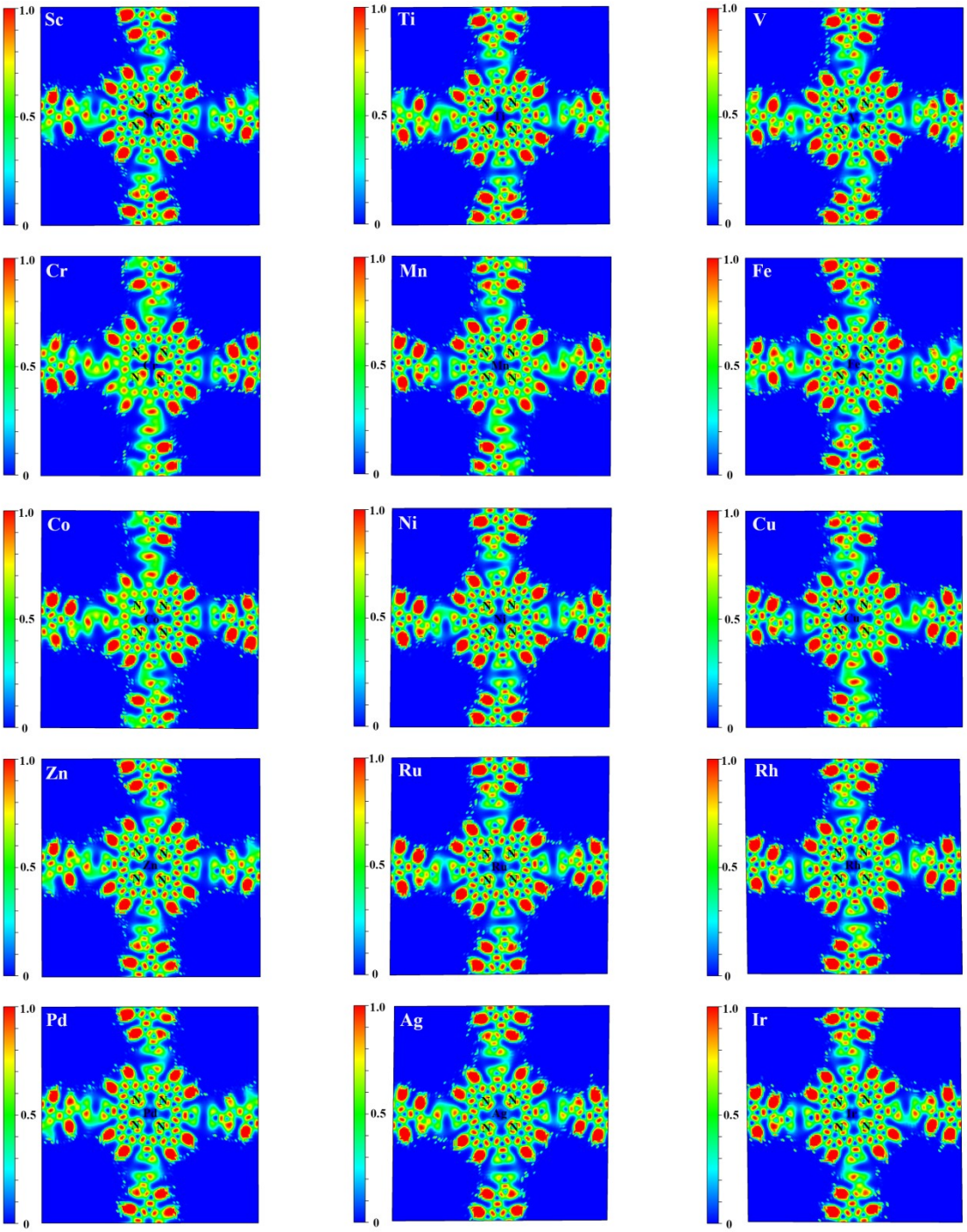


**Fig. S4** Electron localization functions (ELFs) for the metalloporphyrin planes of all the M-COFs.

**Table S1** Standard dissolution potentials ($U^0_{diss}$)[S1] of metal atoms, number of transferred electrons ($n$) during the dissolution, formation energies ($E_{f\text{-}M}$, eV) and calculated dissolution potentials ($U_{diss}$, V vs. SHE) of the metals in M-COFs.

| Metal | $U^0_{diss}$ | $n$ | $E_{f\text{-}M}$ | $U_{diss}$ | Metal | $U^0_{diss}$ | $n$ | $E_{f\text{-}M}$ | $U_{diss}$ |
|---|---|---|---|---|---|---|---|---|---|
| Sc | -2.08 | 3 | -8.32 | 0.69 | Cu | 0.34 | 2 | -3.90 | 2.29 |
| Ti | -1.63 | 2 | -6.03 | 1.38 | Zn | -0.76 | 2 | -5.41 | 1.95 |
| V | -1.18 | 2 | -5.88 | 1.76 | Ru | 0.46 | 2 | -3.30 | 2.11 |
| Cr | -0.91 | 2 | -6.01 | 2.10 | Rh | 0.60 | 2 | -5.46 | 3.33 |
| Mn | -1.19 | 2 | -5.46 | 1.54 | Pd | 0.95 | 2 | -4.92 | 3.41 |
| Fe | -0.45 | 2 | -4.81 | 1.95 | Ag | 0.80 | 1 | -4.27 | 5.07 |
| Co | -0.28 | 2 | -4.77 | 2.11 | Ir | 1.16 | 2 | -4.85 | 3.58 |
| Ni | -0.26 | 2 | -4.96 | 2.22 | | | | | |

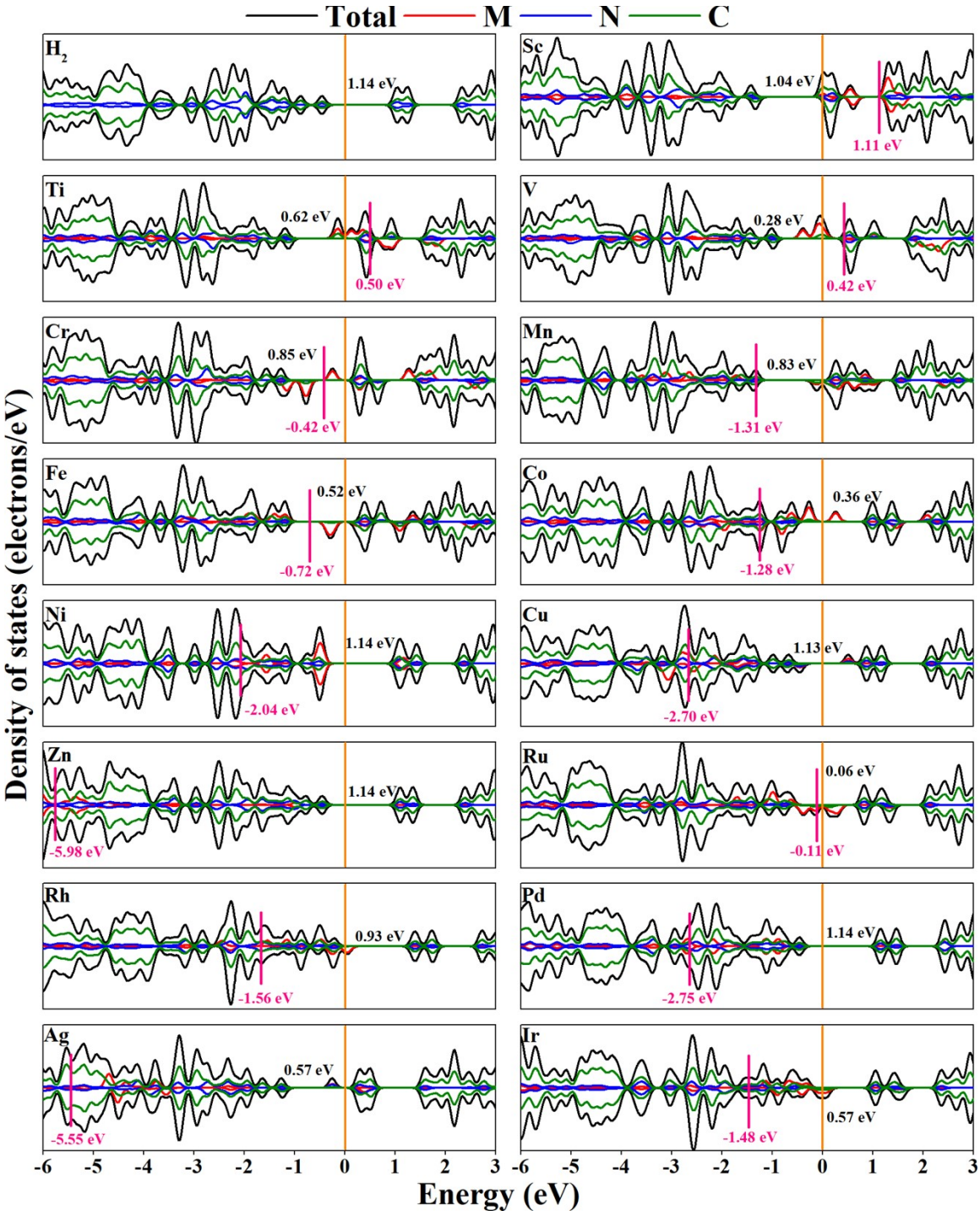


**Fig. S5** Total and projected DOSs of M-COFs with band gap energies (black) and *d*-band centers of the metals (rose). Orange line denotes the Fermi level. Both spin up (top) and spin down (bottom) states are shown.

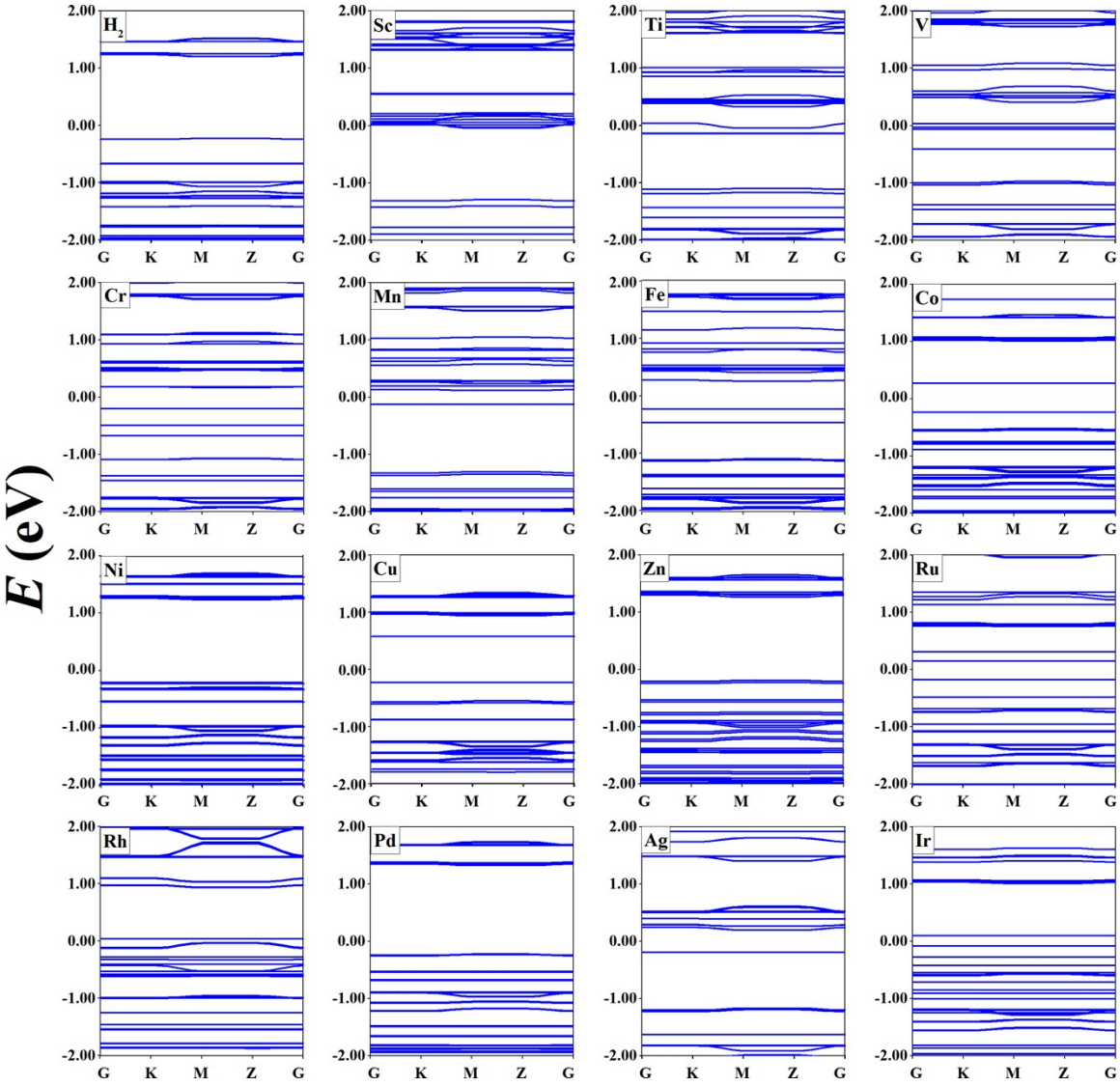


**Fig. S6** Electronic band structures of M-COFs.

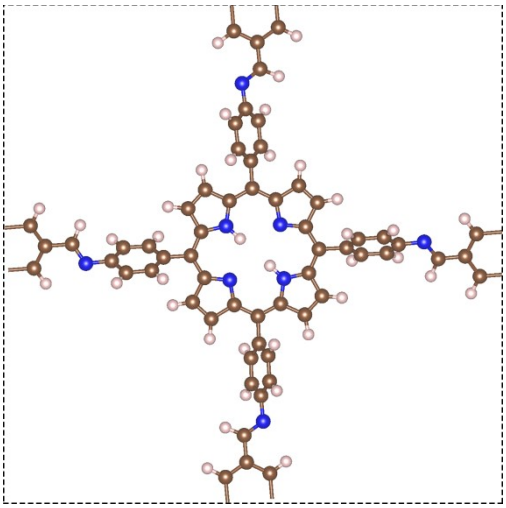

**Fig. S7** Unit cell of the metal-free $H_2$-COFs.

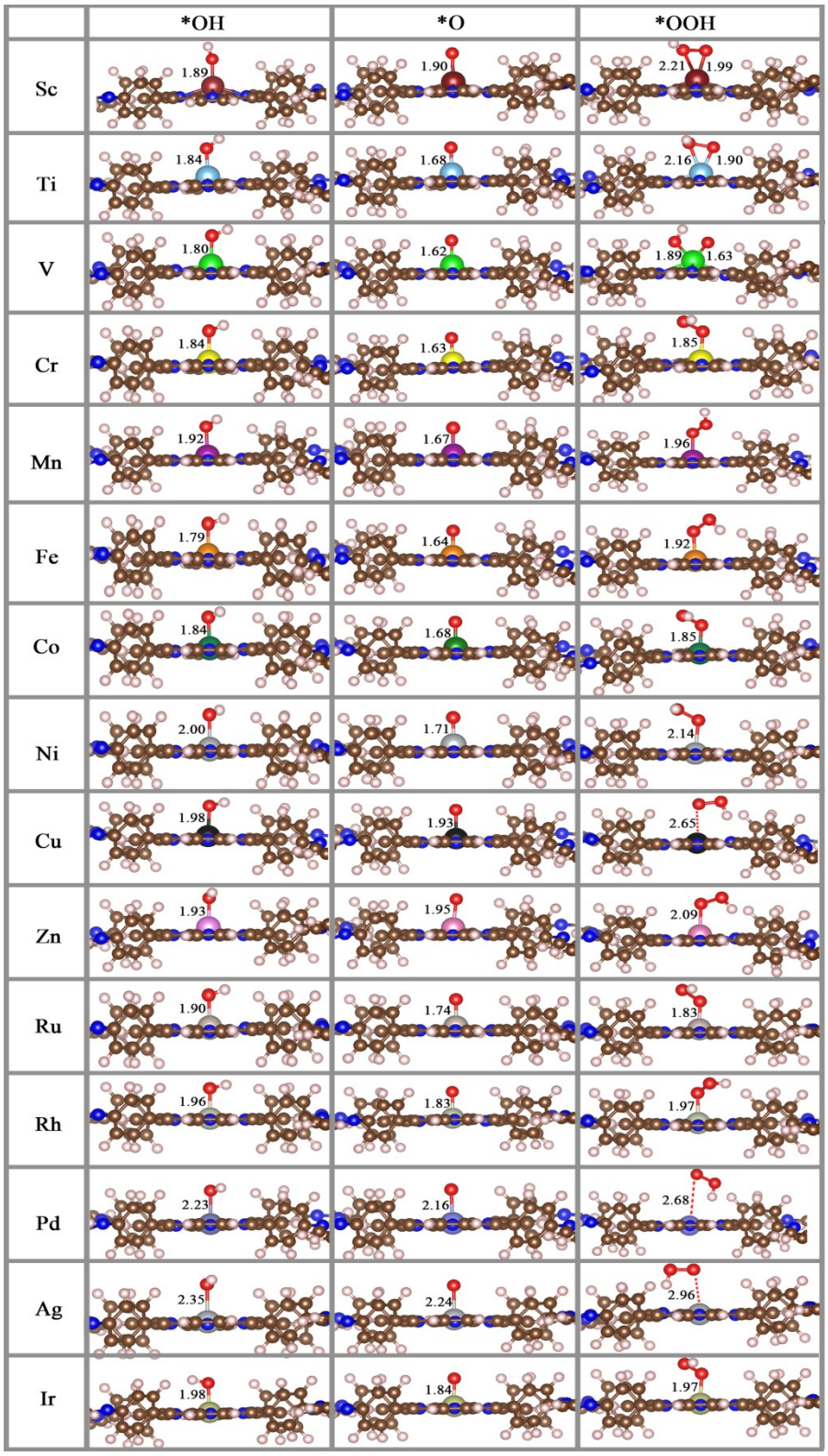


**Fig. S8** Optimized structures of all key intermediate species involved in the OER/ORR process on the M-COFs. The distances are given in Å.

**Table S2** Adsorption free energies of various reaction species on the M-COFs (unit: eV) and OER and ORR overpotentials (V).

| metal | $\Delta G_{*OH}$ | $\Delta G_{*O}$ | $\Delta G_{*OOH}$ | $\eta^{OER}$ | $\eta^{ORR}$ |
|---|---|---|---|---|---|
| Sc | -1.85 | -1.94 | 1.03 | 2.66 | 3.08 |
| Ti | -0.75 | -0.62 | 1.02 | 2.67 | 1.98 |
| V | -0.49 | -0.06 | 1.65 | 2.04 | 1.72 |
| Cr | 0.03 | 2.02 | 3.03 | 0.76 | 1.20 |
| Mn | 1.09 | 2.34 | 4.19 | 0.62 | 0.50 |
| Fe | 1.08 | 2.28 | 4.08 | 0.57 | 0.39 |
| Co | 1.13 | 2.74 | 3.92 | 0.38 | 0.23 |
| Ni | 1.59 | 2.80 | 4.73 | 0.70 | 1.04 |
| Cu | 2.02 | 3.01 | 5.60 | 1.36 | 1.91 |
| Zn | 2.11 | 3.11 | 5.39 | 1.05 | 1.70 |
| Ru | -0.35 | 0.49 | 2.86 | 1.14 | 1.58 |
| Rh | 0.42 | 2.16 | 3.52 | 0.51 | 0.81 |
| Pd | 2.08 | 2.81 | 5.30 | 1.26 | 1.61 |
| Ag | 1.81 | 2.71 | 5.01 | 1.07 | 1.32 |
| Ir | 0.61 | 2.18 | 3.56 | 0.34 | 0.62 |

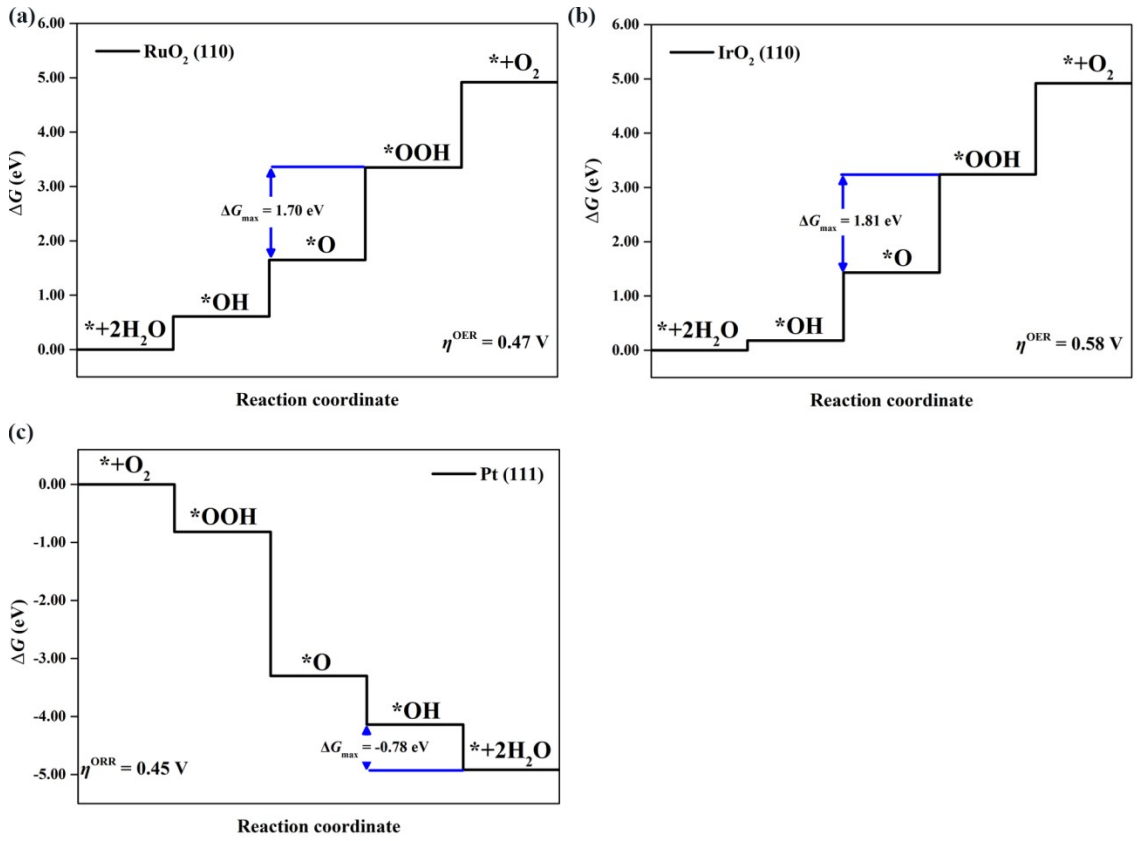


**Fig. S9** Gibbs free energy diagrams for the (a) OER on $RuO_2$ (110) and (b) $IrO_2$ (110) as well as (c) ORR on Pt (111).

Computational Details:

Periodic slab models of the $RuO_2$(110) and $IrO_2$(110) surfaces were constructed by using 2 × 4 surface supercells with three metal oxide layers separated by at least 10 Å of vacuum layer. Periodic slab model of the Pt(111) was constructed using 4 × 4 surface supercells with five metal layers separated by at least 10 Å of vacuum layer. The lattice parameters of $RuO_2$(110), $IrO_2$(110) and Pt(111) are (a = 12.56 Å, b = 12.85 Å, c = 23.14 Å), (a = 12.75 Å, b = 12.86 Å, c = 22.46 Å) and (a = 12.56 Å, b = 11.16 Å, c = 24.06 Å), respectively. The k-points of 2×2×1 was generated by using the Monkhorst-Pack method. The other calculation settings are the same as those for the M-COFs as described in the main text.

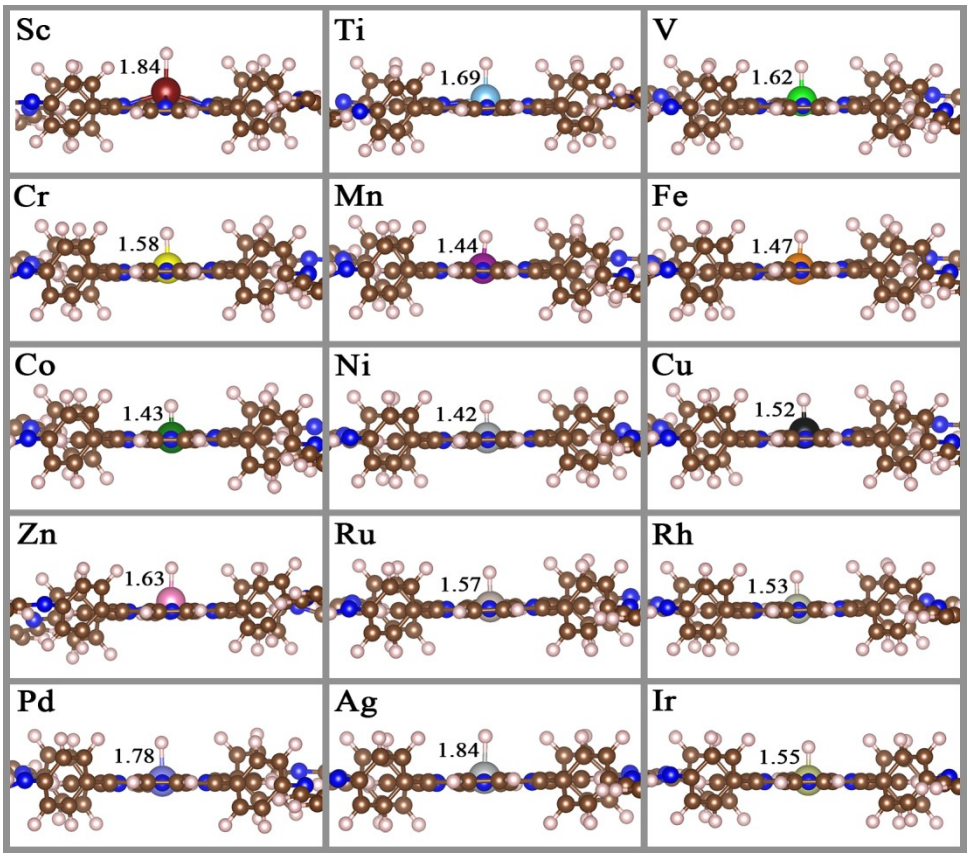


**Fig. S10** Optimized structures of *H intermediates for the HER on the M-COFs. The distances are given in Å.

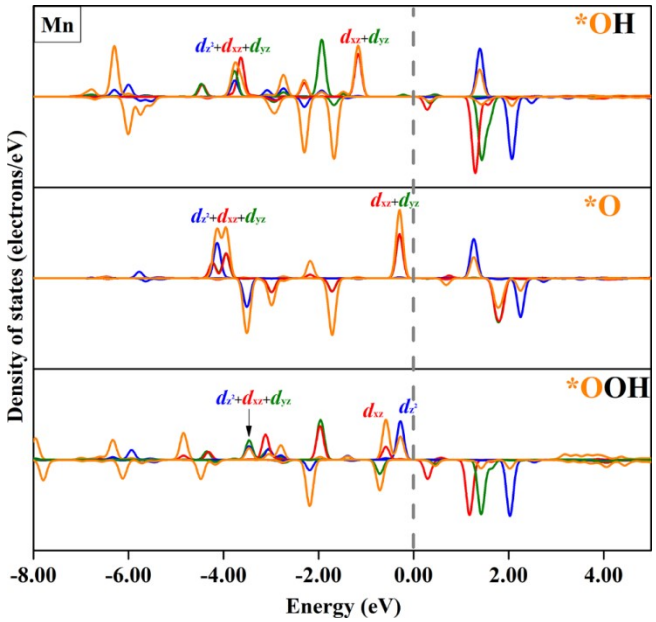


**Fig. S11** PDOSs of axial Mn-3*d* states and O-2*p* states for the OER/ORR intermediates

on Mn-COF (the predominated *d* state is marked if applicable). Both spin up (top) and spin down (bottom) states are shown.

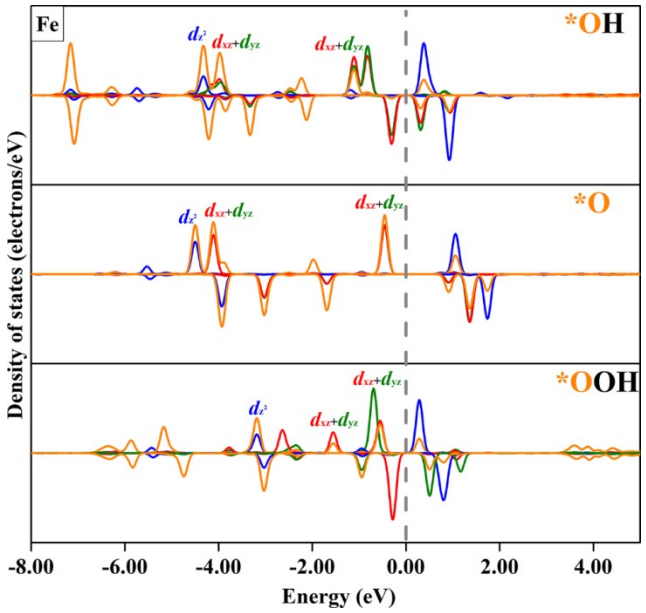


**Fig. S12** PDOSs of axial Fe-3*d* states and O-2*p* states for the OER/ORR intermediates on Fe-COF (the predominated *d* state is marked if applicable). Both spin up (top) and spin down (bottom) states are shown.

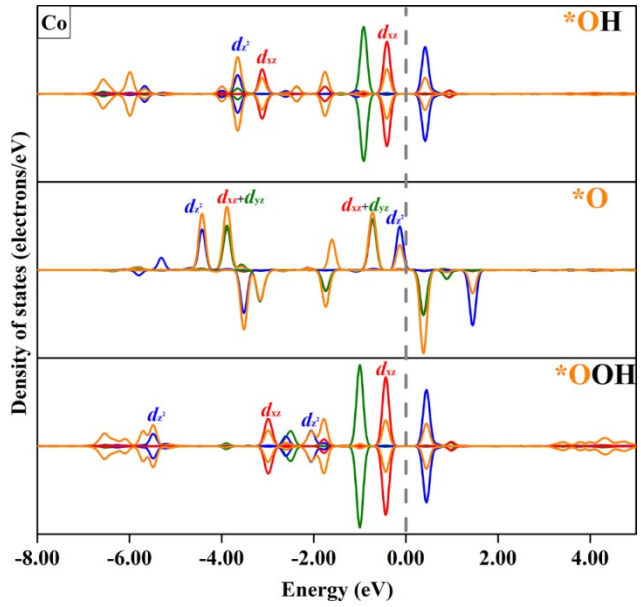


**Fig. S13** PDOSs of axial Co-3*d* states and O-2*p* states for the OER/ORR intermediates on Co-COF (the predominated *d* state is marked if applicable). Both spin up (top) and spin down (bottom) states are shown.

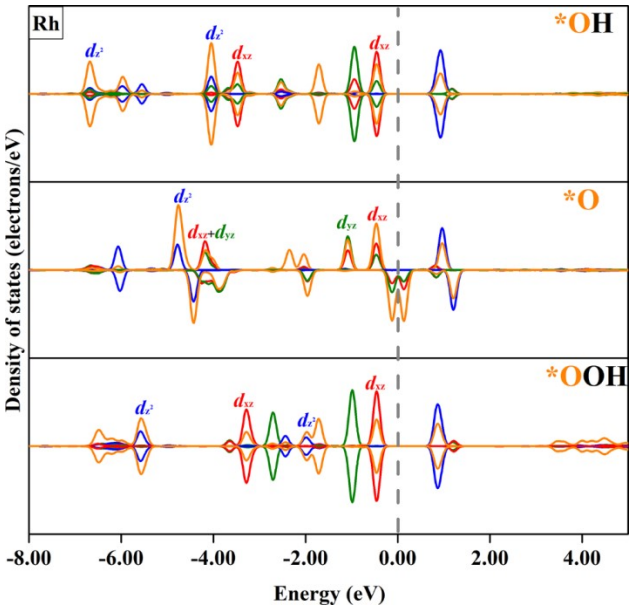


**Fig. S14** PDOSs of axial Rh-4*d* states and O-2*p* states for the OER/ORR intermediates on Rh-COF (the predominated *d* state is marked if applicable). Both spin up (top) and spin down (bottom) states are shown.

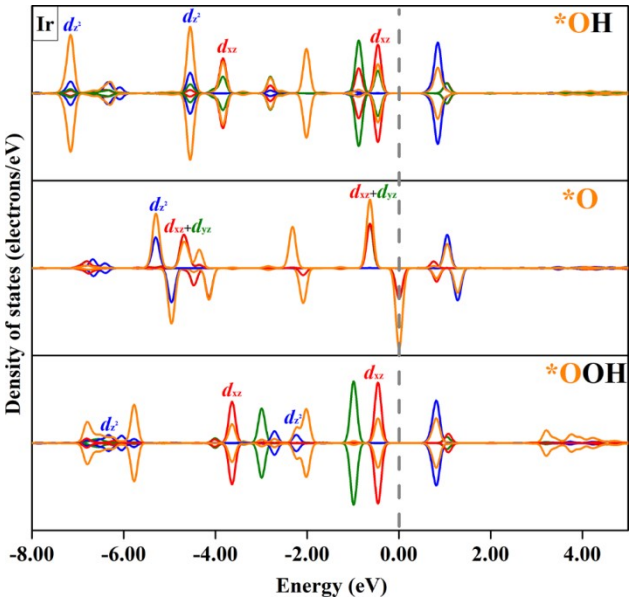


**Fig. S15** PDOSs of axial Ir-5*d* states and O-2*p* states for the OER/ORR intermediates on Ir-COF (the predominated *d* state is marked if applicable). Both spin up (top) and spin down (bottom) states are shown.

## References

S1 X. Guo, J. Gu, S. Lin, S. Zhang, Z. Chen, S. Huang, *J. Am. Chem. Soc.*, 2020, **142**, 5709-5721.